

**Serveur Académique Lausannois SERVAL [serval.unil.ch](http://serval.unil.ch)**

## **Author Manuscript**

**Faculty of Biology and Medicine Publication**

**This paper has been peer-reviewed but does not include the final publisher proof-corrections or journal pagination.**

Published in final edited form as:

**Title:** Dying neurons in thalamus of asphyxiated term newborns and rats are autophagic.

**Authors:** Ginet V, Pittet MP, Rummel C, Osterheld MC, Meuli R, Clarke PG, Puyal J, Truttmann AC

**Journal:** Annals of neurology

**Year:** 2014 Nov

**Volume:** 76

**Issue:** 5

**Pages:** 695-711

**DOI:** 10.1002/ana.24257

In the absence of a copyright statement, users should assume that standard copyright protection applies, unless the article contains an explicit statement to the contrary. In case of doubt, contact the journal publisher to verify the copyright status of an article.

Research Article

**Dying neurons in thalamus of asphyxiated term newborns and rats are autophagic**

Vanessa Ginet<sup>1†</sup>, PhD, Marie P. Pittet<sup>1,2†</sup>, MD, Coralie Rummel<sup>1</sup>, Maria Chiara Osterheld<sup>3</sup>, MD, Reto Meuli<sup>4</sup>, MD, PhD, Peter G.H Clarke<sup>1</sup>, PhD, Julien Puyal<sup>1‡\*</sup>, PhD and Anita C. Truttmann<sup>2‡\*</sup>, MD.

<sup>1</sup>Department of Fundamental Neurosciences, University of Lausanne, Rue du Bugnon 9, CH1005 Lausanne, Switzerland

<sup>2</sup> Clinic of Neonatology, Department of Pediatrics, University Hospital Center, Avenue Pierre Decker 2, CH-1011 Lausanne, Switzerland

<sup>3</sup> Institute of Pathology, University Hospital Center and University of Lausanne, Rue du Bugnon 25, CH-1011 Lausanne, Switzerland

<sup>4</sup> Department of Diagnostic and Interventional Radiology, University Hospital Center and University of Lausanne, Rue du Bugnon 46, CH-1011 Lausanne, Switzerland

†, ‡: These authors contributed equally and should be considered as co-first authors (†) and co-last authors (‡)

\*To whom correspondence should be addressed:

[Anita.Truttmann@chuv.ch](mailto:Anita.Truttmann@chuv.ch) or [JulienPierre.Puyal@unil.ch](mailto:JulienPierre.Puyal@unil.ch);

Running head: **autophagy in asphyxiated newborns**

Number of characters in the title and running head (including space): title (78), running head (33)

Number of words: abstract (243), body of the manuscript (4496)

Number of figures: 8 including 6 color figures

Number of tables: 1

Number of pages: 41

**Acknowledgement statement (including conflict of interest and funding sources):**

We confirm that we have no competing interests to disclose. We thank Jean Daraspe of the Electron Microscopy Facility (University of Lausanne) and the Cellular Imaging Facility (University of Lausanne) for technical and experimental support, and Dr. Céline Fischer for statistical analysis of the human data. This work is dedicated to Prof. Maria Delivoria-Papadopoulos in thanks for her tremendous mentoring of AT. This research was supported by grants from the Swiss National Science Foundation (310030-130769), the Fondation Emma Muschamp and the Faculty of Biology and Medicine (University of Lausanne).

## **ABSTRACT**

**Objective:** Neonatal hypoxic-ischemic encephalopathy (HIE) still carries a high burden by its mortality and long term neurological morbidity in survivors. Apart from hypothermia, there is no acknowledged therapy for HIE, reflecting the lack of mechanistic understanding of its pathophysiology. (Macro)autophagy, a physiological intracellular process of lysosomal degradation has been proposed to be excessively activated in excitotoxic conditions such as HIE. The present study examines whether neuronal autophagy in the thalamus of asphyxiated human newborns or P7 rats is enhanced and related to neuronal death processes.

**Methods:** Neuronal autophagy and cell death were evaluated in the thalamus (frequently injured in severe HIE) of both human newborns who died after severe HIE (n=5) and P7 hypoxic-ischemic rats (Rice-Vannucci model). Autophagic (LC3, p62), lysosomal (LAMP1, cathepsins) and cell death (TUNEL, caspase-3) markers were studied by immunohistochemistry in human and rat brain sections, and by additional methods in rats (immunoblotting, histochemistry and electron microscopy).

**Results:** Following severe perinatal asphyxia in both humans and rats, thalamic neurons displayed up to 10-fold ( $p < 0.001$ ) higher numbers of autophagosomes and lysosomes, implying an enhanced autophagic flux. The highly autophagic neurons presented strong features of apoptosis. These findings were confirmed and elucidated in more detail in rats.

**Interpretation:** These results show for the first time that autophagy is enhanced in severe HIE in dying thalamic neurons of human newborns, as in rats. Experimental neuroprotective strategies targeting autophagy could thus be a promising lead to follow for the development of future therapeutic approaches.

## Introduction

Perinatal asphyxia is a major cause of newborn mortality and long-term neurodevelopmental disabilities, with very limited therapeutic options<sup>1</sup>. Its best known complication is hypoxic-ischemic encephalopathy (HIE), which is characterized by acute neurological impairment, often with seizures and early lesions seen on magnetic resonance imaging (MRI) especially at the level of the perirolandic cortex, the basal ganglia, the thalamus and the brainstem. Twenty five percent of HIE lead to death in the first week of life and up to 50% of survivors develop permanent sequelae such as cerebral palsy, seizures, cognitive and neurosensorial impairment<sup>2</sup>. Despite considerable efforts in research to find clinically safe and effective neuroprotective pharmacotherapy, the only therapy that is currently approved is moderate hypothermia. The heterogeneity of the human hypoxic-ischemic insults and the presence of multiple interacting cell death mechanisms are major difficulties.

Our current understanding of neuronal cell death in human HIE term newborns is very limited because of the lack of human brain studies<sup>3</sup>. One of the most relevant animal models in HIE is a combination of unilateral common carotid artery ligation and exposition to hypoxia on P7 rats<sup>4</sup>, this age being considered comparable to late preterm / term in human brains (34-36 weeks gestation)<sup>5,6</sup>. An important conclusion emerging from studies on rodent perinatal HI is that cell death occurs along an apoptotic-necrotic “continuum”<sup>7</sup> involving predominance of hybrid morphologies of cell death with mixed features of apoptosis and necrosis<sup>8</sup>. However, these may not be the only cell death mechanisms involved, because morphological characteristics of enhanced autophagy have recently been described in the dying neurons<sup>9-11</sup>.

Macroautophagy (hereafter called autophagy) is a physiological degradative process in which cellular components are sequestered in autophagosomes, which fuse with acidic organelles (late endosomes, lysosomes etc.) to form autolysosomes containing the hydrolytic enzymes necessary for the autophagic degradation. Autophagy is essential for maintaining homeostasis and cell survival, but recent studies indicate that it can be involved in cell death, either as a trigger of apoptosis or necrosis, or as an independent mechanism of cell death<sup>12</sup>.

In situations of cerebral HI, the evidence for a death-mediating role of autophagy stems from a combination of morphological and functional evidence. Different studies have demonstrated the presence of enhanced autophagy in dying neurons in neonatal animal models of cerebral ischemia or HI in the cortex and/or hippocampus<sup>9,10,13</sup>. Inhibition of autophagy either pharmacologically<sup>14</sup> or more specifically in neonatal conditional knockout mice with neuron-specific deletion of Atg7<sup>10</sup> is neuroprotective, suggesting a death-mediating role of autophagy.

As the thalamus, including its ventrolateral nucleus (VLNT), is often involved in human HIE, we have studied whether neuronal autophagy is enhanced in the VLNT in brains of human newborns who died from severe HIE and have compared the results with those obtained in a human control group and in the animal model.

## **Materials and Methods**

### ***Rat model of neonatal hypoxia-ischemia***

All experiments were performed in accordance with the Swiss Laws for the protection of animals and were approved by the Vaud Cantonal Veterinary Office. Seven-day old male rats (Sprague Dawley, from Janvier, France) underwent HI (8% of oxygen for 2h) according to the Rice-Vannucci model<sup>4</sup> as previously described<sup>9</sup>. The damage induced by our model of neonatal cerebral HI (2h of hypoxia) was very severe, but with low individual/litter variability in our hands compared to shorter and less severe hypoxic periods (**Fig 1A and 1B**).

### ***Human newborn brain specimens***

Human brain tissues were obtained from 11 deceased and autopsied newborns, provided by the Institute of Pathology, University of Lausanne (**Table 1**). The studied population was selected retrospectively from the death reports of the Clinic of Neonatology (Lausanne University Hospital) between 2001 and 2009. Autopsies were done for medical and legal reasons and informed consent was obtained from the parents. The post mortem interval (time between death and autopsy) was between 5 and 24 hours, and the bodies were conserved in a cold environment. During autopsy, the brain was removed and fixed in 10% buffered formalin for 3 weeks. Samples were then embedded in paraffin and 3µm thick sections were cut. Specimens were then anonymised for research purposes with the approval of the local ethical committee. We selected newborns who died after birth in the context of severe HIE (HIE group, n=5). Death was due to withdrawal of care in 4 cases and due to additional respiratory failure in one case. The criteria for HIE cases were: newborns at or near term (35 to 37 weeks

gestation), with severe perinatal asphyxia, and clinical HIE according to Sarnat grade III<sup>15</sup>. For the control group (n=6), newborns at or near term (35 to 37 weeks of gestation) with life-incompatible conditions were selected (transposition of the great vessels with intact septum (1), primary pulmonary lymphangiectasia (1), congenital diaphragmatic hernia (1), congenital myopathy (2), intrauterine demise with endocardial fibroelastosis (1). Babies with cerebral malformations and genetic anomalies were excluded, as well as babies from whom autoptic material from thalamus was no more available. For comparing the selection criteria between the groups, we calculated the resuscitation score according to Miller et al.<sup>16</sup>.

### ***Cerebral MRI and ADC***

MRI was available for 3 out of 5 HIE cases, using 1.5 or 3 Tesla scanners. Conventional T1 and T2 images and diffusion-weighted images (DWI) were acquired using spin echo echoplanar imaging (SE-EPI), with 5mm thick slices (b values: 0, 500, 1000 mm<sup>2</sup>/s). Apparent diffusion coefficient (ADC) values were calculated from the ADC map choosing similar bilateral regions of interest (ROI) in the VLNT. As reference values we used those published by Rutherford et al.<sup>17</sup>.

### ***Immunoblotting***

Immunoblots on thalamic extracts of sham-operated or HI rat pups were done as described previously<sup>18</sup>. The following primary antibodies were used for protein immunodetection: anti- $\alpha$ -tubulin (sc-8035) mouse monoclonal from Santa Cruz Biotechnology; anti-LC3 (ab48394) rabbit polyclonal from Abcam; anti-active caspase-3

(9661) from Cell Signalling Technology; anti p62/SQSTM1 (P0067) rabbit polyclonal from Sigma-Aldrich and anti-fodrin (FG6090) mouse monoclonal from Biomol (Enzo Life Sciences). Protein bands were visualized using the Odyssey Infrared Imaging System (LI-COR). Odyssey v1.2 software (LI-COR) was used for densitometric analysis. Optical density values were normalized with respect to tubulin and expressed as a percentage of values obtained for sham operated rat pups (100%).

### ***Histochemistry for lysosomal enzymes***

Histochemistry for acid phosphatase and  $\beta$ -N-acetylhexosaminidase was performed on rat pups perfused intracardially with 2% glutaraldehyde and 1% paraformaldehyde in cacodylate buffer (0.1mol/L, pH 7.4) as previously described<sup>9</sup>.

### ***Electron microscopy***

Electron microscopy (EM) was done on rat brains fixed following intracardiac perfusion with 2.5% glutaraldehyde and 2% paraformaldehyde in cacodylate buffer as previously described<sup>14</sup>.

### ***Immunohistochemistry***

For rat tissue, pups were perfused intracardially with 4% paraformaldehyde in 0.1mol/L PBS, pH 7.4. Immunohistochemistry was performed on 18 $\mu$ m cryostat sections as previously described<sup>9</sup>. For human tissue, the paraffin embedded sections were first deparaffinized. After antigen retrieval and blocking in PBS with 15% donkey serum, sections were incubated with primary antibodies in 1.5% donkey serum overnight at 4°C.

For both rat and human sections, Alexa Fluor 488 donkey-anti-rabbit (Invitrogen, A21206) and Alexa Fluor 594 donkey-anti-mouse (Invitrogen, A21203) secondary antibodies were incubated and then sections were mounted with FluoroSave (Calbiochem, 345-789-20) after a Hoechst staining. A LSM 710 Meta confocal microscope (Carl Zeiss) was used for confocal laser microscopy. Confocal images were displayed as individual optical sections. For double-labeling, immunoreactive signals were sequentially visualized in the same section with two distinct filters, with acquisition performed in separated mode. Images were processed with LSM 710 software and mounted using Adobe Photoshop 10.0.

The following primary antibodies were used: anti-LC3 (ab48394, for human) rabbit polyclonal from Abcam; anti-active caspase-3 (9661) rabbit polyclonal from Cell Signalling Technology; anti-cathepsin D (sc-6486, for human) goat polyclonal from Santa Cruz Biotechnology, anti-cathepsin B (06-480) and anti-cathepsin D (06-467, for rat) rabbit polyclonal antibody from Upstate Biotechnology; anti anti-NeuN (MAB377) mouse monoclonal antibody from Chemicon, anti-LAMP1 (428017, for rat) from Calbiochem; anti-GFAP (G3893) mouse monoclonal from Sigma; anti-PGP9.5 (7863-0504) rabbit polyclonal from Bio Trend; anti-LAMP1 (611042, for human) mouse monoclonal from BD Biosciences. Anti-LC3 for rat tissue was a generous gift from Prof. Yasuo Uchiyama (Tokyo, Japan).

### ***TUNEL staining***

After an antigen retrieval for paraffin sections or permeabilization (5 min in 0.2% Triton-X100) for cryostat sections, TUNEL (Terminal deoxynucleotidyl transferase biotin-dUTP Nick End Labeling) staining was performed with DeadEnd Fluorimetric TUNEL system

(Promega, G3250) according to the manufacturer's instructions. For combined immunolabeling, sections were extensively washed in PBS and incubated in primary and secondary antibodies as described above except that pre-incubation of cryostat sections was done without Triton-X100.

### ***Quantification of autophagic and lysosomal labeling***

For rat and human thalamus, confocal images of immunocytochemistry against LC3, cathepsin D, cathepsin B, LAMP1 were acquired using the confocal laser scanning microscope and images were then processed with Adobe Photoshop 10.0. LC3-, cathepsin D- cathepsin B and LAMP1-positive dots were quantified using ImageJ software and expressed as a number of positive dots per neuron per  $\mu\text{m}^2$ . For cathepsin D, cathepsin B and LAMP1-positive dots, dot areas were also quantified using ImageJ software. To quantify autolysosomal areas, we set a lower limit of  $0.5 \mu\text{m}^2$ , in view of the fact that electron microscopical images gave a mean autolysosomal area of  $0.58 \pm 0.28 \mu\text{m}^2$  per neuron.

### ***Statistics***

Biological markers data were expressed as mean  $\pm$  standard deviation (SD). Rat data were derived from at least 3 independent hypoxic-ischemic experiments, corresponding to at least 3 different litters. Data were analyzed statistically using JB STAT software. After testing each group of data for distribution normality (using Shapiro-Wilk tests), we used a multivariate ANOVA for histochemistry to compare rat sham or human control versus rat HI or human HIE values. For immunoblot, in cases of normal distribution, Welch's ANOVA test was followed by a post-hoc Tukey-Kramer test. In the case of a

non-normal distribution, a Kruskal-Wallis test (nonparametric analog of the one-way ANOVA) was followed by a post-hoc Steel-Dwass test to compare the different time points.

The human descriptive data were expressed as median and range, and analyzed using the Statistical Package for Social Science software (SPSS, version 20.0). Univariate analyses of variance, using the Mann-Witney-Wilcoxon and the Fisher's exact tests, were performed.  $p < 0.05$  was chosen as statistically significant.

## Results

### ***Perinatal characteristics of the human population***

Perinatal data and particularly postnatal adaptation from the two groups are represented in **Table 1**. There were no statistical differences between the groups for most of the characteristics such as birth weight, gestational age, gender. As expected, there were significantly more prenatal sentinel events reflected by the significantly lower umbilical artery pH and postnatal seizures in the HIE group than in the control group. The time between birth and death was not statistically different in the two groups, although the median value was higher in the HIE group. In the control group, the babies died between 1h and 28 days after birth (median 13 hours), whereas in the HIE group, the babies died between 20h and 7 days after birth (median 44 hours).

### ***Ventrolateral nucleus thalamus (VLNT) of human neonates and ventrobasal thalamus (VBT) of rat pups are highly vulnerable to hypoxia-ischemia***

In human newborns at term, the predominant neuronal injury pattern after acute and severe asphyxia, known as the “deep nuclear pattern” or “BGT (basal-ganglia-thalamus) pattern” involves the peri-rolandic cortex, the basal ganglia, the thalamus and sometimes the brain stem and hippocampus<sup>19</sup>. But the thalamus, and particularly the VLNT, is especially sensitive to HI<sup>19,20</sup>, so we focused on it, and indeed confirmed this sensitivity. In 3/5 HIE cases, cerebral MRI (T1 and T2) was performed and showed severe thalamic lesions that were confirmed with DWI-ADC as is shown in **Figure 1D**. Diffusion was severely restricted with ADC levels in the ventrolateral thalamus ranging from 0.53 to 0.73 x 10<sup>3</sup>mm<sup>2</sup>/sec (norm values for thalamus 1.0 to 1.1 x 10<sup>3</sup>mm<sup>2</sup>/sec) . Moreover, hematoxylin eosin (HE) staining revealed pyknotic nuclei and cell shrinkage,

confirming neuronal suffering in the VLNT in HIE cases, whereas the control group did not show neuronal injury in the VLNT (**Fig 1E**) or in several other grey matter regions (not shown). Similar histological results were observed for the VBT at 24h in rat pups in our severe model of neonatal cerebral HI (**Fig 1C**).

***Hypoxia-ischemia increases autophagosome abundance in thalamus of both rat pups and human newborns***

In the neonatal rat model, Western blot analyses of thalamic extracts showed that HI caused an increase in the expression of LC3-II, the lipidated form of LC3, which is a marker of autophagosomal membranes (**Fig 2A**). Since the LC3-II expression level was highest at 24h after HI, we decided to focus our investigations on the 24h time point in the rat model.

The effect of HI on autophagy was further investigated by performing immunohistochemistry against LC3. Immunoperoxidase labeling showed a marked increase in the presence of LC3-positive dots (presumably autophagosomes) in the VBT of rats at 6h or 24h after HI, and to some extent at 72h (**Fig 2B**), and in the VLNT of the human HIE cases (**Fig 2C**). The numbers of LC3-positive dots per neuron were then quantified in confocal images of the VBT of HI rat pups and the VLNT of HIE newborns and compared to counts in sham operated rats or human control cases, respectively (**Fig 2D-E**). At 24h after HI in rats, the number of LC3-positive dots per neuron was increased by 6-fold compared to sham-operated animals (**Fig 2D**). Similarly, all human HIE cases displayed an up to 10-fold increase in LC3-positive dots compared to control cases (**Fig 2E**), and this was persistent at 7 days (HIE case 3).

Electron microscopy in HI rat pups revealed that dying VBT neurons displayed marked autophagic characteristics, containing numerous vacuoles, autophagosomes and autolysosomes-like structures in their cytosol (Fig. 3). More specifically, the cell death resembled a recently defined kind of autophagic cell death called autosis<sup>21</sup>, which has been shown to involve sequential phases called 1a, 1b and 2. Each of these phases was represented. Thus, some neurons displayed numerous empty vacuoles, autophagosomes and autolysosomes (arrowheads) in the cytosol, features representative of autosis phase 1a. In others, parts of the perinuclear space were dilated and contained membrane-bound cytosolic regions, the defining characteristic of phase 1b. Still other dying neurons displayed features of phase 2: gross ballooning of parts of the perinuclear space, and the presence of swollen organelles and rupture of the plasma membrane (Fig. 3B). In addition, these dying neurons also showed some morphological characteristics of apoptosis (chromatin condensation, shrinkage of the cytoplasm) and necrosis (observed in phase 2 autosis such as swelling of organelles). These ultrastructural results thus confirmed that HI induced an increase in autophagosomes in neurons from the rat VBT.

***Lysosomal activity and autophagic flux are increased following hypoxia-ischemia in thalamus of rat pups and human newborns***

To evaluate whether the increased number of autophagosomes was due to enhanced autophagic flux (autophagosome formation and autolysosomal degradation after autophagosomes-lysosome fusion) or to failed lysosomal degradation, lysosomal activity was investigated. Immunohistochemistry against different lysosomal markers was performed and the numbers and sizes of positive-dots were quantified. An increased

number of lysosomes, especially of very large lysosomes ( $>0.5\mu\text{m}^2$ ), which are putatively autolysosomes, would reflect an increase in autophagic flux. In neurons in the thalamus of rat pups (**Fig 4A**) and of human newborns (**Fig 4B**) the number of Lysosomal Membrane Protein 1 (LAMP1)-positive vesicles was strongly increased by HI. Moreover, among the positive dots the percentage of larger ones ( $>0.5\mu\text{m}^2$ ), which we assume to represent autolysosomes, increased by 12-fold after HI in rat (**Fig 4C**) and by 8-fold in human HIE (**Fig 4D**). Double immunolabeling against LC3 and LAMP1 showed that neurons with a strong punctate LC3 labeling showed also numerous LAMP1-positive vesicles in HI human newborns (**Fig 4E**) and rat pups (not shown).

Likewise immunohistochemistry against the lysosomal protease cathepsin D (cathD) demonstrated many more cathD-positive dots in HI neurons in both rats (NeuN-positive cells) (**Fig 5A, C**) and humans (PGP9.5-positive cells) (**Fig 5B, D**). Moreover, the size repartition per neuron revealed more than 34% of large dots ( $>0.5\mu\text{m}^2$ ) after HI in rats and more than 28% in humans, whereas in controls the percentage was less than 3% in both rat (**Fig 5C**) and human (**Fig 5D**). Immunolabeling for another lysosomal protease, cathepsin B, gave similar results in the rat HI model (data not shown). These results suggest an increased lysosomal activity following HI.

To verify this, we studied the activity, rather than merely the expression, of two lysosomal enzymes, acid phosphatase (**Fig 6A**) and  $\beta$ -N-acetylhexosaminidase (**Fig 6B**), and found that in each case their activity was enhanced following HI in rat pups, as shown by increased acid phosphatase and  $\beta$ -N-acetylhexosaminidase-positive dots.

To further investigate the change in the level of autophagy, we studied the expression of p62/SQSTM1, a protein selectively degraded by autophagy, by immunoblot on rat extracts<sup>22</sup>. As is shown in **Figure 6C**, p62 expression was

significantly decreased 24h after HI. Immunohistochemistry against p62 confirmed the decrease in p62 expression 24h after HI in rat pups (**Fig 6D**) and also in HI human newborns (**Fig 6E**).

Altogether these results indicate that HI enhances autophagic flux in thalamic neurons in rats and humans.

### ***Enhanced autophagy in relation to neuronal death in thalamus of both rat pups and human newborns***

To investigate the role of the increased neuronal autophagy following HI, we next evaluated the relationships between enhanced autophagy and cell death, focusing on the activation of caspase-3 as a marker of apoptosis and using DNA fragmentation and morphology as additional markers of cell death.

In rat pups we showed by immunoblotting that cerebral HI increases progressively the expression levels both of cleaved caspase-3 and of the caspase-dependent cleavage product (120kDa) of  $\alpha$ -fodrin from 6h to at least 72h after HI (**Fig 7A**). Immunohistochemistry for cleaved caspase-3 clearly confirmed the activation of caspase-3 in rat VBT (**Fig 7B**), where DNA fragmentation was also detected by TUNEL staining (**Fig. 8A, B**). In human newborns we likewise showed caspase-3 activation (**Fig 7C**) and TUNEL labeling (**Fig 8C**) after HI whereas the controls were always negative for both caspase-3 (**Fig. 7C, E**) and TUNEL staining (**Fig. 8C**).

As apoptotic and autophagic processes share several regulators and as autophagy has been shown to trigger caspase-3 activation in cerebral HI, we evaluated the level of autophagy in caspase-3 positive neurons by quantifying the number and size

of LAMP1 positive vesicles in rat (**Fig 7D**) and human (**Fig 7E**). Double labeling experiments revealed that many thalamic neurons positive for cleaved caspase-3 presented a strong punctate LAMP1 staining suggesting that the two mechanisms occur in the same neurons in HI rat and human HIE brains. Similar results were obtained with TUNEL stain in the rat model 24h after HI (**Fig 8B**) and in human HIE brains (**Fig 8C**).

Altogether, these results reveal that autophagy is enhanced in dying neurons of human VNL and rat VBT.

## **Discussion**

The present study was designed to investigate the possibility of enhanced neuronal autophagy in severe perinatal HIE in human newborns and to validate the clinical relevance of results obtained by our group and others in experimental HI rodent models. We previously demonstrated that HI in P7 rats enhances neuronal autophagy in CA3 hippocampal and cortical dying neurons<sup>8,21</sup>. Moreover, in a similar HI mouse model, the specific inhibition of autophagy through neuron-specific deletion of the autophagy-related gene *Atg7* conferred resistance to hippocampal neurons<sup>10</sup> providing a strong argument for a death-mediating role of autophagy in rodent neonatal HI.

Our human brain specimens came from autopsied newborns who died in the context of severe hypoxic-ischemic encephalopathy. It was therefore logical to relate the human results to those from an animal model that is likewise severe. The present neonatal HI rodent model, proposed by Vannucci 30 years ago<sup>4</sup>, has become the standard model and has allowed several deleterious cellular pathways to be identified<sup>3</sup>. One conclusion has been that excitotoxic and HI-induced neuronal death in immature brains occurs across a spectrum ranging from apoptosis to necrosis<sup>7</sup>, but the situation has been complicated by evidence for multiple interacting neuronal death mechanisms<sup>3,23</sup> including a death-mediating role of enhanced autophagy in different brain regions of neonatal rodents after HI<sup>8,9,24,25</sup>.

### ***Neuronal autophagy is enhanced in neurons of human VLNT after HI***

We here report for the first time the presence of enhanced autophagy in dying neurons after HI in human newborns. We compared to tissues from newborns who died due to other life-incompatible conditions, where no enhanced autophagy could be

detected. The main differences between the HIE and the control groups resided in the fact that all HIE cases presented sentinel events affecting them already just before birth. The control group presented a compromised postnatal adaptation due mainly to respiratory insufficiency. Supported by our data from the rat model, we can conclude that autophagic flux, meaning autophagosome formation and autolysosomal degradation, is increased in VLNT human neurons.

First, all HIE cases display an increased number of LC3-positive vesicles compared to control cases. After conjugation to phosphatidylethanolamine (PE), LC3 is converted to the LC3-II form and recruited to the autophagosomal membrane until its degradation by lysosomal hydrolases. Quantification of LC3-positive dots is considered one of the most reliable methods for evaluating autophagosome abundance<sup>26</sup>. Other complementary strategies are the measure of LC3-II expression level after immunoblotting and the identification of multimembrane compartments surrounding cytoplasmic materials including organelles by electron microscopy. The latter two techniques were not possible on the human brain samples but were performed on rat pup brains confirming that neonatal HI increases autophagosomal numbers in the rat VBT.

To confirm an enhanced autophagic flux, it is essential to demonstrate that increased autophagosome abundance occurs along with a higher level of lysosomal clearing since a defect in degradation would result in autophagosome accumulation. After human and rat neonatal HI, lysosomal vesicles labeled with LAMP1, cathD and/or cathB were not only more numerous but also larger in thalamic neurons containing abundant autophagosomes (LC3-positive dots), indicating a greater autophagic lysosomal activity with increased presence of autolysosomes. This hypothesis was

strengthened by our results on the rat model showing degradation of the autophagy substrate p62 and enhanced activity of two lysosomal enzymes in VBT after HI. In both rat and human thalamic neurons, p62 immunolabeling confirmed that p62 was apparently reduced and certainly not accumulated following HI. Several studies have shown enhanced neuronal autophagy in diverse *in vitro*<sup>27,28</sup> and *in vivo*<sup>29,30</sup> models of excitotoxicity including adult and neonatal cerebral HI<sup>9,10,13,14,31-35</sup>.

### ***The enhanced autophagy occurs in dying neurons of human VLNT after HI***

Our results also show, in both humans and rats, that many of the neurons expressing enhanced autophagy were dying, since many of them were positive for activated caspase-3 and for TUNEL. In humans, very few post-mortem neuropathological studies of neonatal HIE are available, and most described only necrotic-like cell death<sup>36</sup>, although a few did mention the presence of apoptosis in the cerebral cortex and basal ganglia<sup>3</sup>. Our results make it clear that apoptotic-like cell death with apoptotic (but also necrotic) features including caspase-3 activation did occur in VLNT. This was yet another point of resemblance between the human and the rodent neuropathologies. Several rodent studies have described related results in cerebral ischemia in both adults<sup>29,31,34</sup> and neonates<sup>9,10</sup>. However, in our neonatal HI rat model the relationships with apoptosis can be region-dependent since strong autophagy is activated simultaneously with apoptosis in cortical neurons whereas in the degenerating hippocampus CA1 neurons are purely apoptotic (not autophagic) and CA3 neurons are purely autophagic (not apoptotic)<sup>9</sup>. The neuronal cell death induced by HI in the thalamus of rat pups is thus more comparable to that occurring in the cortex. In such cases, with autophagy and apoptosis activated in the same neuron, the autophagy may

perhaps trigger an apoptotic execution, as has been shown in the death of cortical neurons exposed to different apoptotic stimulations<sup>18</sup>.

Both human and animal studies have demonstrated sexual dimorphism in neonatal cerebral hypoxia/ischemia<sup>37-40</sup>. It has been shown that there is sex-specific activation of cell death signaling pathways. For example cell death in females occurs mainly via a caspase-dependent pathway whereas in males caspase-independent pathways (AIF, PARP) seem to be more important players<sup>41-43</sup>. We currently work only with male rat pups to avoid any possible gender differences in signaling. However, in the human data we were obliged to use both genders because of the scarcity of available brain tissue. However when the HI insult is severe in rodents, there are no significant sex differences in the extent of brain damage<sup>41</sup> (**Fig 1B**) or in the level of LC3-II expression (not shown)<sup>41</sup>.

We did not, however, address the function of the neuronal autophagy in the present study. Enhanced autophagy can be related to cell death in different ways. Its best known function is a protective reaction to maintain cell survival as has been described in nutrient deprivation or pathogen invasion<sup>44-46</sup>. It can also be just an epiphenomenon or, at the other extreme, an active player in the cell death machinery. Evidence for a detrimental role in cerebral ischemia is currently much stronger than that for a protective one<sup>23</sup>. In particular, strong evidence for a death-promoting role of autophagy has been deduced in several cerebral ischemia models from the neuroprotective effects of its inactivation, achieved not only by pharmacological means in numerous papers<sup>11,14,47</sup>, but also by the specific knock-down of autophagy genes in adult cerebral ischemia<sup>35</sup> or their specific deletion in a conditional knockout model of neonatal HI<sup>10</sup>. We recently demonstrated that downregulation of the autophagy-related

protein Beclin1 reduced the striatal lesion in the same hypoxic-ischemic rodent model as in the present experiments<sup>48</sup>. Our data corroborate the study of Koike and colleagues (2008) showing that the hippocampus becomes resistant in mice when another autophagy-related gene, Atg7, is specifically inhibited in neurons after mild hypoxia-ischemia<sup>10</sup>. Moreover we recently showed that cardiac glycosides such as neriifolin were able to inhibit a form of autophagic cell death, designated autosis, that occurs in the present model<sup>21</sup>. Our present results indicate that the neuronal death in the thalamus resembles autosis but has features of apoptosis as well. Of particular interest, neonatal hypoxic–ischemic brain damage and autophagy in rat were both strongly reduced by treatment with neriifolin in both cortex and thalamus<sup>21</sup>. In cases where neuronal enhanced autophagy promotes cell death, the cellular pathways involved can be various. It can trigger necrosis<sup>49,50</sup> but more often apoptosis<sup>18,51-53</sup>. We previously demonstrated that some widely used apoptotic stimuli can activate autophagy flux in primary cortical neurons with a strong contribution to caspase-dependent (caspase-3 activation) and -independent (AIF nuclear translocation) apoptosis<sup>18</sup>. In specific conditions, autophagy can also be a cell death mechanism by itself, independently of apoptosis or necrosis<sup>12,19,54-56</sup>. Due to its described paradoxical roles, the function of enhanced autophagy in cell death is still a subject of debate<sup>12,57</sup>.

In conclusion we have shown for the first time that autophagy is enhanced in thalamic neurons of human newborns with HIE as well as in a rodent model of severe perinatal asphyxia. We hypothesize, based on experimental results on different rodent models of cerebral ischemia, that autophagy could be involved in triggering neuronal death in the human HIE. Experimental neuroprotective strategies targeting autophagy

could then be a promising lead to follow for the development of future therapeutic approaches.

### **Authorship and contributorship**

All authors have contributed substantially to this research study. VG performed experiments on animal and human tissue, analysis of the data and wrote much of the manuscript, MPP performed experiments on human tissue, analyzed the data and wrote much of the manuscript , CR performed parts of experiments, MCO participated in selecting human tissue and revised the manuscript, RM participated in description and analysis of the MR-images of the newborns and revised the manuscript, PGHC helped in designing the study and revised the manuscript, JP and ACT designed and supervised the experiments and were involved in the writing of the manuscript.

## Figure legends

**Table 1: Descriptive data of the human population.** There was a significant difference ( $p < 0.05$ ) between the two groups for the Apgar score at 1 minute, the initial umbilical arterial pH, the frequency of secondary apnea and of postnatal seizures. Interestingly, the resuscitation score according to Miller et al.<sup>15</sup> was not different between the groups, strengthening the choice of the control group. The data is expressed as median and range, or in some cases ratio and percentage because of the small numbers. Some information such as Apgar score, secondary apnea and seizures are missing for one control case. †one missing information. \*according to Miller score<sup>15</sup>. § $p < 0.05$  statistically significant.

**Figure 1. Perinatal asphyxia induces severe neuronal injury in the thalamus of both rat and human neonates.**

**(A)** Representative images of coronal brain sections stained with cresyl violet showing the evolution of the lesion as sampled at four time-points: 6h, 24h, 72h and 1 week (w) after hypoxia-ischemia (HI). Bar = 1 cm. **(B)** Quantification of damaged brain tissue 24 h after the insult induced by 2h of hypoxia in P7 male and female rats shows a severe but reproducible lesion. No significant difference in the percentage of total damaged tissue relative to the contralateral hemisphere was found between males ( $74 \pm 4\%$ ,  $n=11$ ) and females ( $70 \pm 8\%$ ,  $n=11$ ). Values are mean $\pm$ SD. **(C)** Hematoxylin-eosin (HE) stains reveal that the rat ventro-basal thalamus is strongly affected by perinatal HI 24h after the insult with the presence of cell shrinkage and pyknotic nuclei. Black rectangles

correspond to the higher magnifications in the ventro-basal thalamus. Bar = 200 $\mu$ m for the low resolution (left panel) and 50  $\mu$ m for the higher magnifications (middle and right panels). **(D)** Cerebral MR-imaging with T2-weighted, diffusion and ADC (apparent diffusion coefficient) maps obtained in HIE-cases **1(a1-3)**, **2(b1-3)** and **3(c1-3)**. Top row shows transverse T2-weighted images at 34 hours (a), 40 hours (b) and 48 (c) hours after birth, respectively; middle row shows the diffusion-weighted images (DWI) at the same times and bottom row represents the ADC maps. **a1**: absence of signal anomaly in thalamus, basal ganglia and in cortex on T2-weighted images, but **a2** presents a restricted diffusion in thalamus (arrow) bilaterally as well as the corticospinal tract and both hippocampi (not seen here), confirmed on ADC maps (arrow **a3**). **b1** shows a severe diffuse cerebral edema with hyperintensity in thalamus/basal ganglia and loss of differentiation between gray and white matter for global cortex, seen also on the DWI (**b2**) with restricted diffusion on the thalamus (short arrow) and global cortex (long arrow) and confirmed on ADC maps (**b3**). **c1** shows no anomaly on this image, but additional corticospinal tract hyperintensities were seen on adjacent images. **c2 shows** restricted diffusion bilaterally in the posterior limb of the internal capsule (PLIC), and ventrolateral thalamus; restricted diffusion occurred also in the corticospinal tract (not in this image, but in adjacent ones). This was confirmed on ADC maps (**c3**). The mean ADC values measured on the right and left ventrolateral nucleus of the thalamus (VLNT), were strongly reduced in all 3 HIE cases, confirming cytotoxic edema in VLNT bilaterally. **(E)** Representative images showing that dying neurons in the VLNT of HIE cases display cell shrinkage and pyknotic nuclei as shown using a hematoxylin-eosin (HE) stain compared to control cases. Bar = 20 $\mu$ m.

**Figure 2. Hypoxia-ischemia increases the number of neuronal autophagosomes in the thalamus of both rat and human neonates. (A)** Representative immunoblots and the corresponding quantification of LC3-II expression after HI in rat pups, demonstrating a persistent increase in autophagosomes peaking at 24h (6h:  $116 \pm 20\%$ ,  $n=13$ , 24h:  $176 \pm 42\%$   $n=16$ , 48h:  $146 \pm 34\%$ ,  $n=17$ , 72h:  $149 \pm 31\%$ ,  $n=10$ , 1 week (w):  $156 \pm 22\%$ ,  $n=8$ ) compared to sham operated animals (sham P8:  $100 \pm 6\%$ ,  $n=11$ , sham P14:  $128 \pm 11\%$ ,  $n=7$ ). Values are mean  $\pm$  SD and are expressed as a percentage of sham P8 value. \* $p < 0.05$ , \*\* $p < 0.01$ , \*\*\*  $p < 0.001$ . Steel-Dwass test. **(B)** Representative LC3 immunoperoxidase labeling in the ventrobasal thalamus of rat pups at different time points indicating an increase in LC3-positive dots after hypoxia-ischemia (HI). High magnifications of a representative neuron in sham-operated rat and 24h after HI are shown. Bars =  $20\mu\text{m}$ . **(C)** Representative LC3 immunoperoxidase labeling in the ventrolateral thalamus of human newborns illustrating the increase in LC3 expression in hypoxic-ischemic encephalopathy (HIE) cases compared to control. High magnification shows punctate labeling in the HIE case. Bar =  $20\mu\text{m}$ . **(D)** Representative confocal images of neurons in ventrobasal thalamus of rat pups and quantification of LC3-positive dots (red) in neuronal autophagosomes showing an increase (24h HI:  $0.278 \pm 0.069$ ; sham:  $0.046 \pm 0.018$  LC3-positive dots/neuron/ $\mu\text{m}^2$ ) at 24h after HI. The quantification was performed on neurons labelled with NeuN (green) in 5 rats (20 neurons/rat). Bar =  $20\mu\text{m}$ . **(E)** Representative confocal images of neurons in ventro-lateral thalamus of human newborns, and quantifications. Left graph: numbers of LC3-positive dots in the 6 control and 5 hypoxic-ischemic encephalopathy (HIE) cases shown individually. Right graph: average numbers of LC3-positive dots in control ( $0.028 \pm 0.003$ ) and HIE ( $0.328$

$\pm 0.035$ ) cases. Bar = 50 $\mu$ m. n  $\geq$  50 neurons/case. Nuclei are stained with Hoechst (in blue). Values are mean  $\pm$  SD. \*\* p < 0.01, \*\*\* p < 0.001. Welch ANOVA.

**Figure 3. Neonatal HI-induced neuronal death in the rat thalamus with autophagic characteristics.**

**(A)** Representative electron micrographs of neurons in sham-operated rat pups (right panel) and 24h after HI (middle and left panels) showing numerous multimembrane vacuoles (presumably autophagosomes) containing cytoplasmic material as illustrated at high magnifications. Bars = 1 $\mu$ m and 0.5 $\mu$ m for higher magnifications. m = mitochondrion, GA = Golgi apparatus and ER = endoplasmic reticulum. **(B)** Electron microscopic analyses revealed that dying neurons in the thalamus showed morphological features of autosis ("autophagic cell death"). Some dying neurons displayed numerous empty vacuoles, autophagosomes (asterisks) and autolysosomes (arrowheads) in the cytosol representative of autosis phase 1a. Others exhibited swollen parts of the perinuclear space containing membrane-bound cytosolic regions (arrows, phase 1b). Then, some dying neurons displayed features of phase 2 autosis: focal ballooning of the perinuclear space, swollen organelles and rupture of the plasma membrane. In addition, these dying neurons also showed some morphological characteristics of apoptosis (chromatin condensation, shrinkage of the cytoplasm) and necrosis (observed in phase 2 autosis such as swelling of organelles). N: nucleus, INM: inner nuclear membrane, ONM: outer nuclear membrane; PNS: perinuclear space.

**Figure 4. Hypoxia-ischemia in the thalamus of both rat and human neonates increases the number and size of LAMP1-positive vesicles. (A-B)** Representative

immunoperoxidase labeling of LAMP1 illustrating the increase in its expression after hypoxia-ischemia in rats (HI) **(A)** and in human HIE cases **(B)**. High magnifications of a representative neuron are shown in each case. At 72h after HI, the positive labeling probably corresponds mainly to macrophages, as is suggested by the cellular morphology. Bar = 20 $\mu$ m. **(C)** Confocal images of LAMP1 expression (green) in neurons labeled with MAP2 (red), near the periphery of the lesion in HI rat pups. Quantification of these data shows increases in the number of dots/neuron/ $\mu$ m<sup>2</sup> (left histogram) (sham: 0.065  $\pm$  0.018, 24h HI: 0.302  $\pm$  0.077) and in the percentage of large dots with respect to all dots (right histogram) (sham: 2.6  $\pm$  1.3%, 24h HI: 33.6  $\pm$  3.3%) in rat pups 24h after hypoxia-ischemia (HI). n=5 rats (20 neurons/rat). **(D)** A similar analysis showing a strong increase of LAMP1 dots in neurons in human HIE cases. The two histograms on the left represent the number of dots/neuron/ $\mu$ m<sup>2</sup> (upper) and the percentage of large dots (>0.5 $\mu$ m<sup>2</sup>) (lower) in the 6 control and the 5 hypoxic-ischemic encephalopathy (HIE) cases shown individually. The histograms on the right represent the average numbers. Human newborns with severe HIE display far more LAMP1-positive dots (control: 0.033  $\pm$  0.022, HIE: 0.261  $\pm$  0.05) and with a much higher proportion of large vesicles (control: .4.2  $\pm$  1.9%, HIE: 32.2  $\pm$  5%). **(E)** Double immunolabeling against LAMP1 (in green) and LC3 (in red) in human newborn brain sections reveals that in HIE cases neurons with strong autophagic features display also numerous putative autolysosomes (shown by numerous large LAMP1-positive dots). Nuclei are stained with Hoechst (in blue). Bar = 20 $\mu$ m.

**Figure 5. Hypoxia-ischemia in the thalamus of both rat and human neonates increases the number and size of cathepsin D-positive vesicles. (A-B)**

Representative immunoperoxidase labeling of Cathepsin D (CathD) illustrating the increase in CathD expression after hypoxia-ischemia in rats (HI) (A) and in human HIE cases (B). High magnifications of a representative neuron are shown in each case. At 72h after HI, the positive labelling probably corresponds mainly to macrophages as is suggested by the cellular morphology. Bar = 20 $\mu$ m. Confocal images of CathD expression (red) in neurons labelled in green with (C) NeuN for rats or (D) PGP9.5 for humans. Quantification of these data shows increases in the numbers of CathD dots. (C) In the rat HI model, the numbers of dots/neuron/ $\mu$ m<sup>2</sup> (upper graph) are  $0.039 \pm 0.009$  for sham and  $0.112 \pm 0.031$  for 24h HI. The percentage of dots  $>0.5\mu$ m<sup>2</sup> with respect to all dots are  $2.6 \pm 1\%$  for sham and  $34.4 \pm 4\%$  for 24h HI. Nuclei are stained with Hoechst (in blue). (D) For human HIE the two histograms on the left represent the number of dots/neuron/ $\mu$ m<sup>2</sup> (upper) and the percentage of large dots with respect to all dots ( $>0.5\mu$ m<sup>2</sup>) (lower) in the 6 control and 5 hypoxic-ischemic encephalopathy (HIE) cases shown individually. The two histograms on the right represent the average numbers. Human newborns with severe HIE display far more cathD-positive dots (control:  $0.033 \pm 0.007$ , HIE:  $0.166 \pm 0.026$ ) with a much higher proportion of large vesicles (control:  $4.3 \pm 1\%$ , HIE:  $28.6 \pm 4\%$ ).  $n \geq 50$  neurons/case. Values are mean  $\pm$  SD. \*\*\*  $p < 0.001$ . Welch ANOVA. Bar = 20 $\mu$ m.

**Figure 6. Lysosomal activity is enhanced by cerebral hypoxia-ischemia in the thalamus of both rat and human neonates.** Histochemistry for the activity of (A) acid

phosphatase (AP) and **(B)**  $\beta$ -N-acetylhexosaminidase shows an increase in the number of positive dots. Bar = 20 $\mu$ m. **(C)** Representative immunoblots for p62/SQSTM1 and the corresponding quantification, showing that p62 expression in the rat thalamus is significantly reduced 24h after hypoxia-ischemia (HI) (sham: 100  $\pm$  7%, n = 9; 24h HI: 65  $\pm$  17%, n = 8). Values are mean  $\pm$  SD and are expressed as a percentage of sham value. \*\*\* p < 0.001. Welch ANOVA. **(D-E)** Representative confocal images of p62 (in green) and lysosomal markers (LAMP1 and cathepsin D (cathD) in red) **(D)** in the rat HI model and **(E)** in human newborns with severe hypoxic-ischemic encephalopathy (HIE) confirming that HI induces a decrease in p62 expression (and no p62 accumulation) in neurons displaying strong autophagic features. Nuclei are stained with Hoechst (in blue). Bar = 20 $\mu$ m.

**Figure 7. Caspase-3 positive neurons are highly autophagic in the thalamus of both rat and human neonates after hypoxia-ischemia.** **(A)** Representative immunoblots for cleaved caspase-3 and  $\alpha$ -fodrin in rat thalamic extracts and the corresponding quantifications demonstrate that hypoxia-ischemia (HI) triggers caspase-3 activity as shown by an increase in both its cleaved active form (17kDa) (6h: 671  $\pm$  477%; 24h: 2135  $\pm$  1325%; 48h: 2826  $\pm$  1502%; 72h: 3236  $\pm$  2430%) and the caspase-3-dependent cleavage of  $\alpha$ -fodrin (120kDa) (6h: 153  $\pm$  49, 24h: 388  $\pm$  295%; 48h: 438  $\pm$  326%; 72h: 448  $\pm$  236%) (Steel-Dwass test). Immunoblots for  $\alpha$ -fodrin also indicate an HI-induced activation of calpains as suggested by the high level of the calpain-dependent cleavage product (150kDa) (6h: 766  $\pm$  487%; 24h: 1268  $\pm$  573%, 48h: 1259  $\pm$  494%; 72h: 1037  $\pm$  841%) (Tukey-Kramer test). Values are mean  $\pm$  SD. \*p < 0.05, \*\*\* p < 0.001. **(B)** Representative images of immunoperoxidase labeling against cleaved

caspase-3 confirm a strong activation of caspase-3 after HI in the rat ventro-basal thalamus at 6, 24 and 72h. **(C)** Peroxidase immunohistochemistry against cleaved caspase-3 (in brown) followed by a Nissl stain (in purple) reveals that human HIE brains expressed numerous caspase-3-positive neurons (arrows) with highly condensed and pyknotic nuclei (high magnification) compared to control newborns. Bar = 20 $\mu$ m. **(D-E)** Confocal images showing LAMP1 (in green) and cleaved caspase-3 (in red) distribution and the corresponding quantifications illustrating that caspase-3 positive neurons show a high number of LAMP1-positive dots (upper graph) with a strong proportion of large ones ( $>0.5\mu\text{m}^2$ ) (lower graph) in both **(D)** the ventro-basal thalamus of rat pups 24h after hypoxia-ischemia (HI) and **(E)** the ventrolateral thalamus of human newborns with severe hypoxic-ischemic encephalopathy (HIE cases, n=5). The numbers of LAMP1-positive dots ( $0.29 \pm 0.1$  dots/ $\mu\text{m}^2$  for rat;  $0.23 \pm 0.09$  dots/ $\mu\text{m}^2$  for human) and the percentage of dots  $>0.5\mu\text{m}^2$  ( $32 \pm 9\%$  for rat;  $27 \pm 10\%$  for human) per neuron expressing cleaved caspase-3 are not significantly different ( $p>0.05$ ) from the average values obtained in overall neurons after HI ( $0.30 \pm 0.08$  dots/ $\mu\text{m}^2$  and  $34 \pm 3\%$  for rat;  $0.26 \pm 0.05$  dots/ $\mu\text{m}^2$  and  $36 \pm 3\%$  for human). Nuclei are stained with Hoechst (in blue). Values are mean  $\pm$  SD. Welch ANOVA.  $n \geq 20$  neurons per rat or per human case. Bars = 20 $\mu$ m.

**Figure 8. TUNEL-positive neurons are highly autophagic in the thalamus of both rat and human neonates after hypoxia-ischemia.** **(A)** Representative images of peroxidase revelation of TUNEL staining following HI demonstrate that neonatal HI strongly increases the number of TUNEL-positive cells at 24h after HI. Black rectangles

correspond to the higher magnifications in the ventro-basal thalamus. Bar = 100 $\mu$ m. **(B)** Confocal images of LAMP1 expression (in red) combined with a TUNEL stain (in green) and corresponding quantifications demonstrate that TUNEL-positive neurons of the rat ventro-basal thalamus 24h after hypoxia-ischemia (HI) show an increased number of LAMP1-positive dots (upper graph,  $0.33\pm 0.14$  dots/ $\mu\text{m}^2$ ) with a strong percentage of large dots ( $>0.5\mu\text{m}^2$ ) (lower graph,  $26.43\pm 12.09\%$ ) which are not statistically different compared to the overall HI neurons ( $0.30\pm 0.08$  and  $34\pm 3\%$  respectively). Bar = 20 $\mu$ m. Nuclei are stained with Hoechst (in blue). **(C)** Confocal images showing cathepsin D (cathD, in red) combined with a TUNEL stain (in green) and the corresponding quantifications demonstrating that TUNEL-positive neurons in the ventrolateral thalamus of human newborns show numerous cathD-positive dots (upper graph,  $0.18\pm 0.03$  dots/ $\mu\text{m}^2$ ) with a strong proportion of large ones ( $>0.5\mu\text{m}^2$ ) (lower graph,  $26.57\pm 7.45\%$ ) in severe hypoxic-ischemic encephalopathy (HIE cases, n=5), although the numbers are not statistically different ( $p>0.05$ ) from the average value obtained in overall neurons after HI ( $0.16 \pm 0.03$  dots/ $\mu\text{m}^2$  and  $28.57 \pm 3.71\%$  respectively). Values are mean  $\pm$  SD. Welch ANOVA. n  $\geq$  20 neurons/rat or case. Bars = 20 $\mu$ m.

## References

1. Edwards AD, Brocklehurst P, Gunn AJ et al. Neurological outcomes at 18 months of age after moderate hypothermia for perinatal hypoxic ischaemic encephalopathy: synthesis and meta-analysis of trial data. *British Medical Journal*. 2010; 340
2. Okerefor A, Allsop J, Counsell SJ et al. Patterns of brain injury in neonates exposed to perinatal sentinel events. *Pediatrics*. 2008; 121:906-914
3. Northington FJ, Chavez-Valdez R, Martin LJ. Neuronal Cell Death in Neonatal Hypoxia-Ischemia. *Ann Neurol*. 2011; 69:743-758
4. Rice JE, Vannucci RC, Brierley JB. The Influence of Immaturity on Hypoxic-Ischemic Brain-Damage in the Rat. *Ann Neurol*. 1981; 9:131-141
5. Romijn HJ, Hofman MA, Gramsbergen A. At what age is the developing cerebral cortex of the rat comparable to that of the full-term newborn human baby? *Early Hum Dev*. 1991;26(1):61-7.
6. Northington FJ. Brief update on animal models of hypoxic-ischemic encephalopathy and neonatal stroke. *Ilar Journal*. 2006; 47:32-38
7. Portera-Cailliau C, Price DL, Martin LJ. Excitotoxic neuronal death in the immature brain is an apoptosis- necrosis morphological continuum. *J Comp Neurol*. 1997; 378:70-87
8. Northington FJ, Ferriero DM, Graham EM et al. Early neurodegeneration after hypoxia-ischemia in neonatal rat is necrosis while delayed neuronal death is apoptosis. *Neurobiol Dis*. 2001; 8:207-219

9. Ginet V, Puyal J, Clarke PGH et al. Enhancement of autophagic flux after neonatal cerebral hypoxia-ischemia and its region-specific relationship to apoptotic mechanisms. *Amer J Pathol.* 2009; 175:1962-1974
10. Koike M, Shibata M, Tadakoshi M et al. Inhibition of autophagy prevents hippocampal pyramidal neuron death after hypoxic-ischemic injury. *Amer J Pathol.* 2008; 172:454-469
11. Puyal J, Ginet V, Grishchuk Y et al. Neuronal Autophagy as a Mediator of Life and Death: Contrasting Roles in Chronic Neurodegenerative and Acute Neural Disorders. *Neuroscientist.* 2012; 18:224-236
12. Clarke PGH, Puyal J. Autophagic cell death exists. *Autophagy.* 2012; 8(6):867-9.
13. Zhu C, Wang X, Xu F et al. The influence of age on apoptotic and other mechanisms of cell death after cerebral hypoxia-ischemia. *Cell Death Differ.* 2005; 12:162-176
14. Puyal J, Vaslin A, Mottier V et al. Postischemic treatment of neonatal cerebral ischemia should target autophagy. *Ann Neurol.* 2009; 66:378-389
15. Sarnat HB, Sarnat MS. Neonatal Encephalopathy Following Fetal Distress - Clinical and Electroencephalographic Study. *Archives of Neurology.* 1976; 33:696-705
16. Miller SP, Weiss J, Barnwell A et al. Seizure-associated brain injury in term newborns with perinatal asphyxia. *Neurology.* 2002; 58:542-548

17. Rutherford M, Biarge MM, Allsop J et al. MRI of perinatal brain injury. *Pediatric Radiology*. 2010; 40:819-833
18. Grishchuk Y, Ginet V, Truttmann AC et al. Beclin 1-independent autophagy contributes to apoptosis in cortical neurons. *Autophagy*. 2011; 7:1115-1131
19. de Vries LS, Groenendaal F. Patterns of neonatal hypoxic-ischaemic brain injury. *Neuroradiology*. 2010; 52:555-566
20. Krageloh-Mann I, Helber A, Mader I et al. Bilateral lesions of thalamus and basal ganglia: origin and outcome. *Developmental Medicine and Child Neurology*. 2002; 44:477-484
21. Liu Y, Shoji-Kawata S, Sumpter RM Jr, Wei Y, Ginet V, Zhang L, Posner B, Tran KA, Green DR, Xavier RJ, Shaw SY, Clarke PG, Puyal J, Levine B. Autosis is a Na<sup>+</sup>,K<sup>+</sup>-ATPase-regulated form of cell death triggered by autophagy-inducing peptides, starvation, and hypoxia-ischemia. *Proc Natl Acad Sci U S A*. 2013;110(51):20364-71.
22. Ichimura Y, Kumanomidou T, Sou YS, Mizushima T, Ezaki J, Ueno T, et al. Structural basis for sorting mechanism of p62 in selective autophagy. *The Journal of biological chemistry*. 2008; 283(33):22847-57.
23. Puyal J., Ginet V., and Clarke P.G.H. Multiple interacting cell death mechanisms in the mediation of excitotoxicity and ischemic brain damage: A challenge for neuroprotection. *Progress in Neurobiology* . 2013. 105:24-48.

24. Nakajima W, Ishida A, Lange MS et al. Apoptosis has a prolonged role in the neurodegeneration after hypoxic ischemia in the newborn rat. *J Neurosci*. 2000; 20:7994-8004
25. Sheldon RA, Hall JJ, Noble LJ et al. Delayed cell death in neonatal mouse hippocampus from hypoxia-ischemia is neither apoptotic nor necrotic. *Neurosci Lett*. 2001; 304:165-168
26. Klionsky DJ, 1269 others. Guidelines for the use and interpretation of assays for monitoring autophagy. *Autophagy*. 2012; 8(4):445-544
27. Borsello T, Croquelois K, Hornung JP et al. N-methyl-D-aspartate-triggered neuronal death in organotypic hippocampal cultures is endocytic, autophagic and mediated by the c-Jun N-terminal kinase pathway. *Eur J Neurosci*. 2003; 18:473-485
28. Matyja E, Taraszewska A, Naganska E et al. Autophagic degeneration of motor neurons in a model of slow glutamate excitotoxicity in vitro. *Ultrastruct Pathol*. 2005; 29:331-339
29. Piras A, Gianetto D, Conte D et al. Activation of Autophagy in a Rat Model of Retinal Ischemia following High Intraocular Pressure. *Plos One*. 2011; 6(7):e22514.
30. Shacka JJ, Lu J, Xie ZL et al. Kainic acid induces early and transient autophagic stress in mouse hippocampus. *Neurosci Lett*. 2007; 414:57-60
31. Adhami F, Liao GH, Morozov YM et al. Cerebral ischemia-hypoxia induces intravascular coagulation and autophagy. *Amer J Pathol*. 2006; 169:566-583

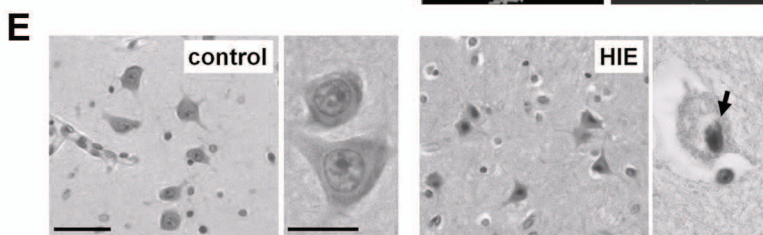
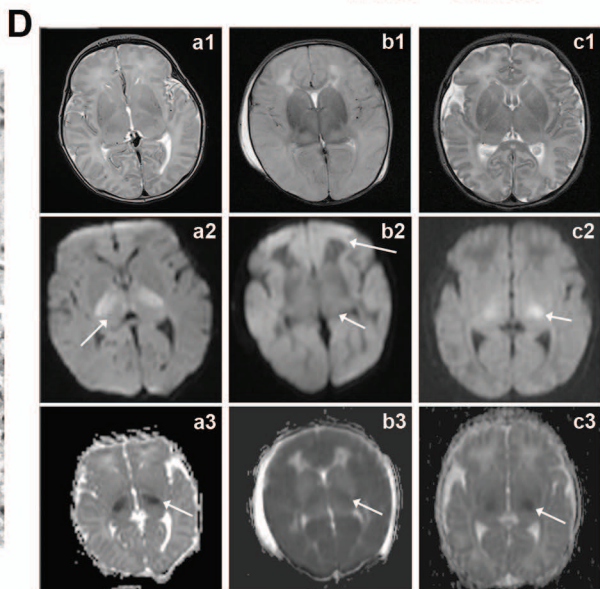
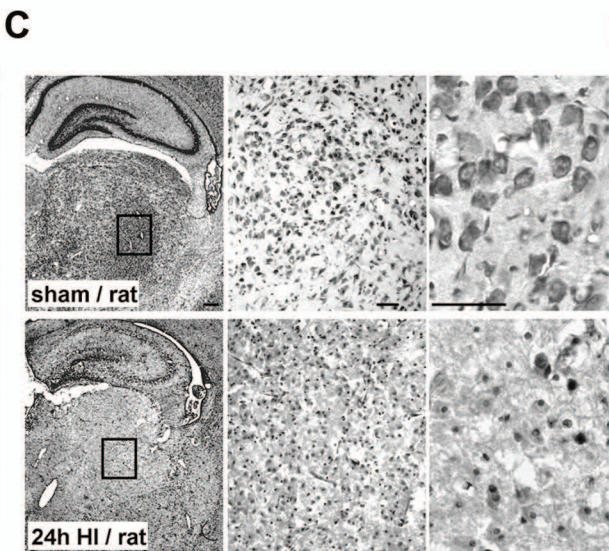
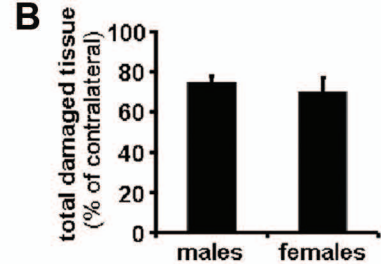
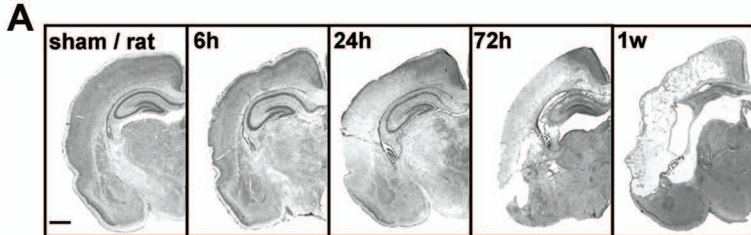
32. Gao L, Jiang T, Guo J et al. Inhibition of Autophagy Contributes to Ischemic Postconditioning-Induced Neuroprotection against Focal Cerebral Ischemia in Rats. *Plos One*. 2012; 7
33. Nitatori T, Sato N, Kominami E et al. Participation of cathepsins B, H, and L in perikaryal condensation of CA1 pyramidal neurons undergoing apoptosis after brief ischemia. *Adv Exp Med Biol*. 1996; 389:177-185
34. Rami A, Langhagen A, Steiger S. Focal cerebral ischemia induces upregulation of Beclin 1 and autophagy-like cell death. *Neurobiol Dis*. 2008; 29:132-141
35. Xing SH, Zhang YS, Li JJ et al. Beclin 1 knockdown inhibits autophagic activation and prevents secondary neurodegenerative damage in the ipsilateral thalamus following focal cerebral infarction. *Autophagy*. 2012; 8:63-76
36. Takizawa Y, Takashima S, Itoh M. A histopathological study of premature and mature infants with pontosubicular neuron necrosis: Neuronal cell death in perinatal brain damage. *Brain Research*. 2006; 1095:200-206
37. Alkayed NJ, Harukuni I, Kimes AS et al.. D. Gender-linked brain injury in experimental stroke. *Stroke*. 1998. 29:159-165
38. Hurn PD, Vannucci S J and Hagberg H. Adult or perinatal brain injury - Does sex matter? *Stroke*. 2005. 36:193-195
39. Vagnerova K, Koerner IP and Hurn PD. Gender and the injured brain. *Anesthesia and Analgesia*. 2008. 107:201-214

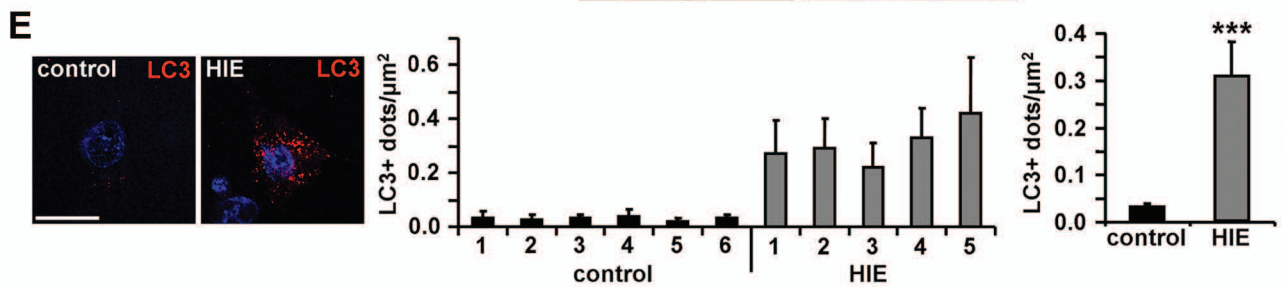
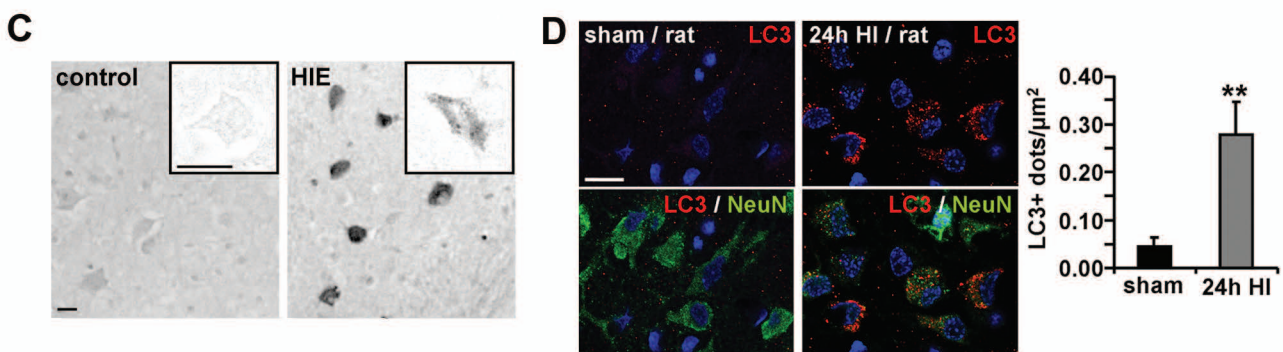
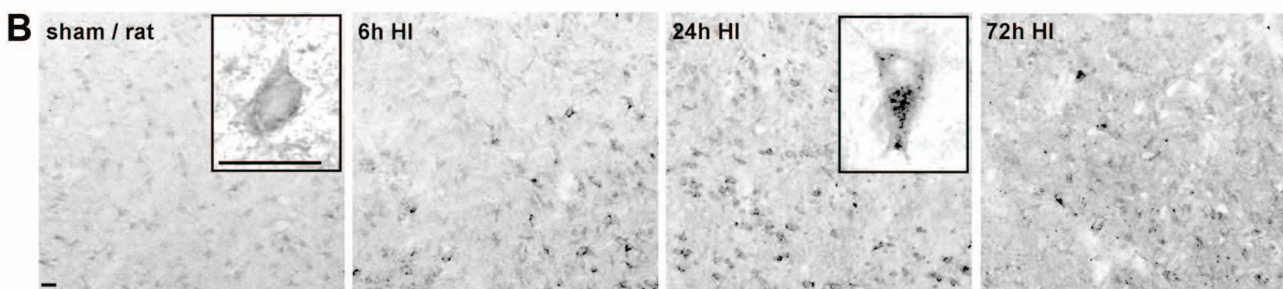
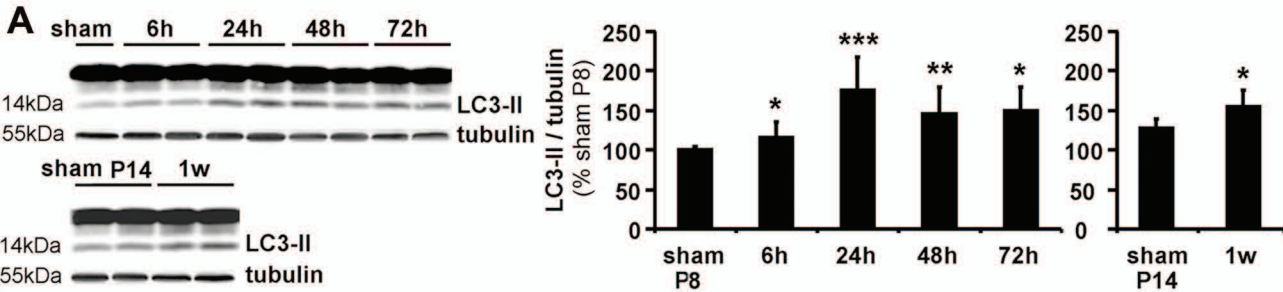
40. Turtzo LC and McCullough LD. Sex-specific responses to stroke. *Future Neurol.* 2010. 5:47-59
41. Zhu CL, Xu FL, Wang XY et al. Different apoptotic mechanisms are activated in male and female brains after neonatal hypoxia-ischaemia. *Journal of Neurochemistry.* 2006. 96:1016-1027
42. Lang JT and McCullough LD. Pathways to ischemic neuronal cell death: are sex differences relevant? *J. Translat. Med.* 2008. 6:33
43. Renolleau S, Fau S and Charriaut-Marlangue C. Gender-related differences in apoptotic pathways after neonatal cerebral ischemia. *Neuroscientist.* 2008. 14:46-52.
44. Kuma A, Hatano M, Matsui M et al. The role of autophagy during the early neonatal starvation period. *Nature.* 2004; 432:1032-1036
45. Liang XH, Kleeman LK, Jiang HH et al. Protection against fatal Sindbis virus encephalitis by Beclin, a novel Bcl-2-interacting protein. *Journal of Virology.* 1998; 72:8586-8596
46. Mizushima N. Role of mammalian autophagy as a starvation response. *Molecular Biology of the Cell.* 2004; 15:242A
47. Wen YD, Sheng R, Zhang LS et al. Neuronal injury in rat model of permanent focal cerebral ischemia is associated with activation of autophagic and lysosomal pathways. *Autophagy.* 2008; 4:762-769

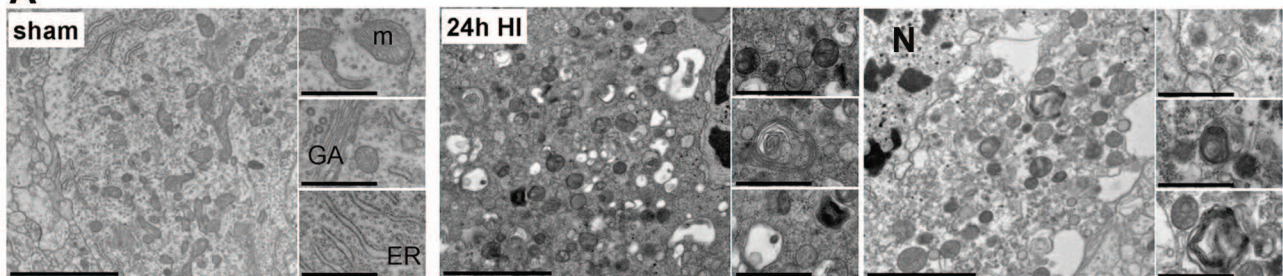
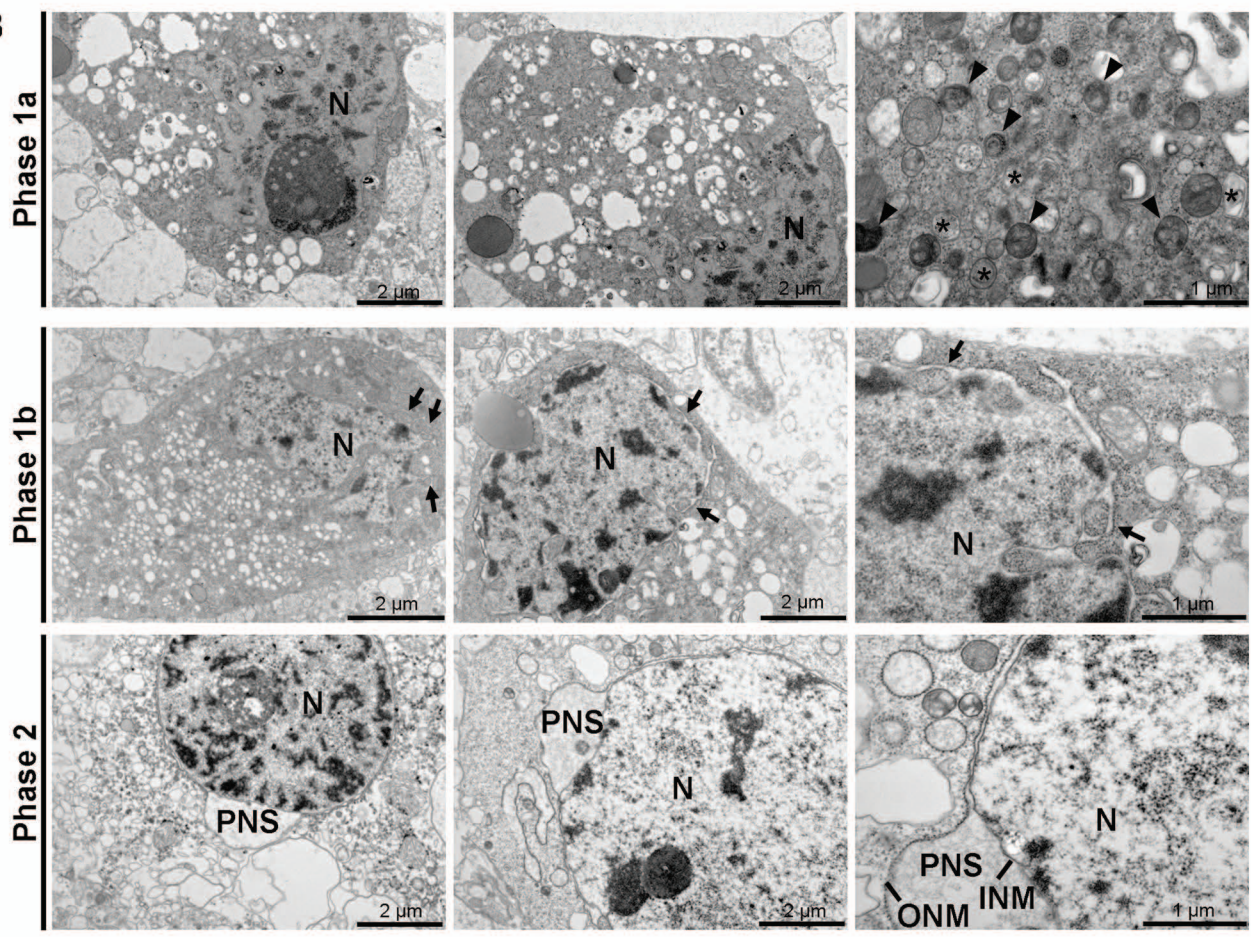
48. Ginet V, Spiehlmann A, Rummel C, Rudinskiy N, Grishchuk Y, Luthi-Carter R, Clarke PG, Truttmann AC and Puyal J. Involvement of autophagy in hypoxic-excitotoxic neuronal death. *Autophagy*. 2014. 11:10(5):846-60.
49. Samara C, Syntichaki P, Tavernarakis N. Autophagy is required for necrotic cell death in *Caenorhabditis elegans*. *Cell Death Differ*. 2008; 15:105-112
50. Wang JY, Xia QA, Chu KT et al. Severe Global Cerebral Ischemia-Induced Programmed Necrosis of Hippocampal CA1 Neurons in Rat Is Prevented by 3-Methyladenine: A Widely Used Inhibitor of Autophagy. *Journal of Neuropathology and Experimental Neurology*. 2011; 70:314-322
51. Dong XX, Wang YR, Qin S et al. P53 Mediates Autophagy Activation and Mitochondria Dysfunction in Kainic Acid-Induced Excitotoxicity in Primary Striatal Neurons. *Neuroscience*. 2012; 207:52-64
52. Xue LZ, Fletcher GC, Tolkovsky AM. Autophagy is activated by apoptotic signalling in sympathetic neurons: An alternative mechanism of death execution. *Molec Cell Neurosci*. 1999; 14:180-198
53. Zhang XD, Wang Y, Wang Y et al. p53 mediates mitochondria dysfunction-triggered autophagy activation and cell death in rat striatum. *Autophagy*. 2009; 5:339-350
54. Clarke PGH. Developmental cell death: morphological diversity and multiple mechanisms. *Anat Embryol (Berl)*. 1990; 181:195-213

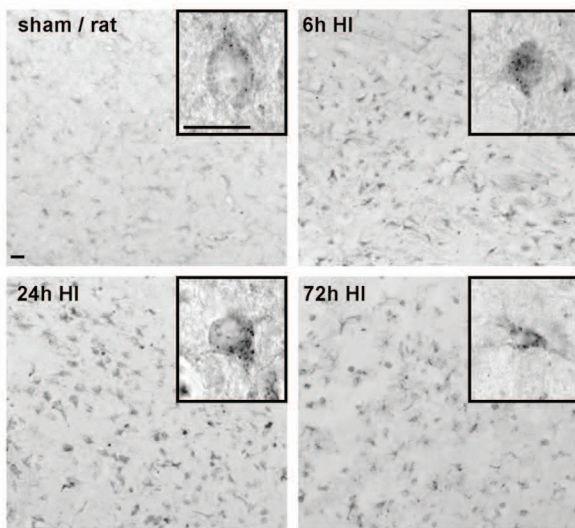
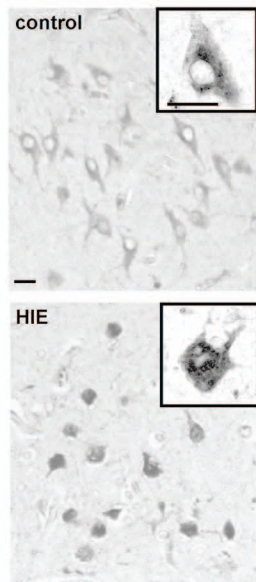
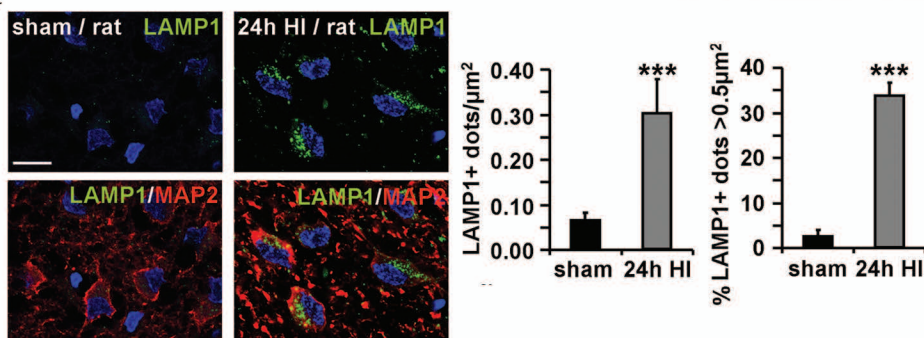
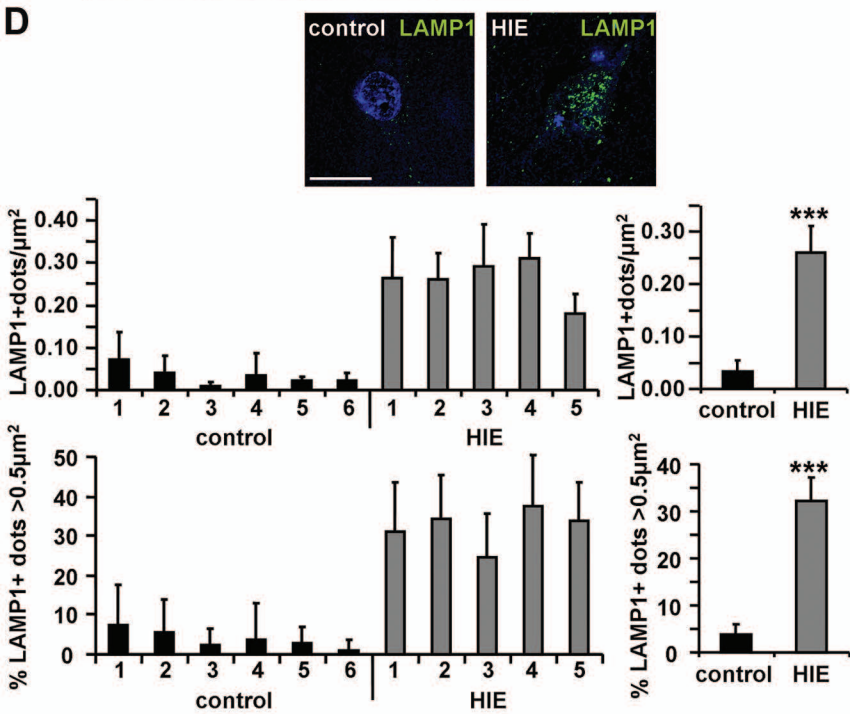
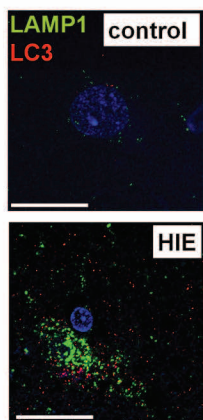
55. Denton D, Shrivage B, Simin R et al. Autophagy, Not Apoptosis, Is Essential for Midgut Cell Death in *Drosophila*. *Curr Biol*. 2009; 19:1741-1746
56. Luciani MF, Giusti C, Harms B et al. Atg1 allows second-signaled autophagic cell death in *Dictyostelium*. *Autophagy*. 2011; 7:501-508
57. Kroemer G, Levine B. Autophagic cell death: the story of a misnomer. *Nature Rev Molec Cell Biol*. 2008; 9:1004-1010

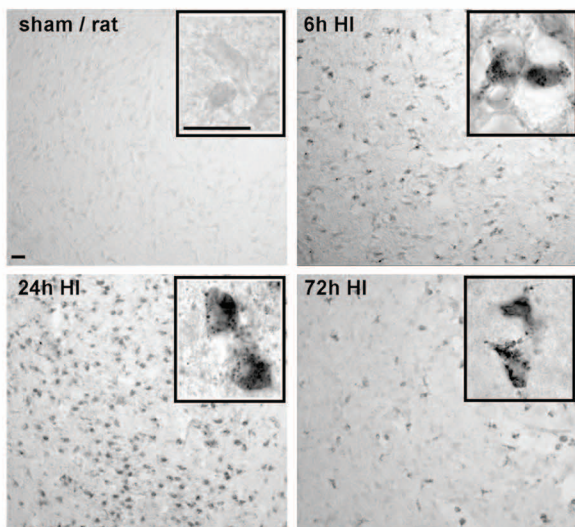
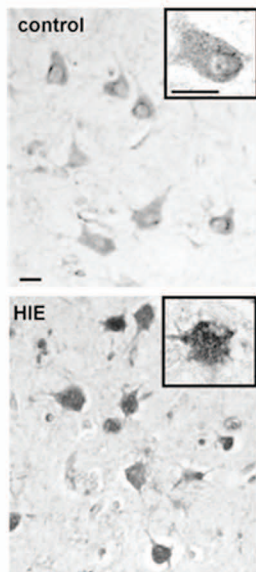
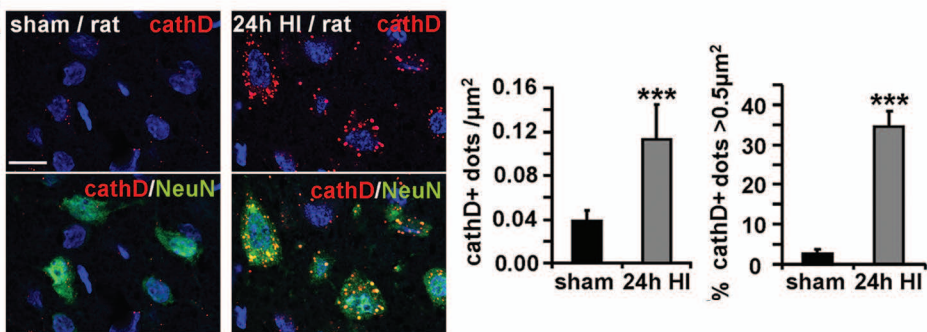
<b>Groups</b>	<b>HIE (n=5)</b>	<b>Control (n=6)</b>	<b>p values</b>
<b>Gestational age (days)</b>			
<b>median</b>	<b>277</b>	<b>272.5</b>	<b>0.712</b>
<b>range</b>	<b>268-287</b>	<b>250-290</b>	
<b>Birthweight (g)</b>			
<b>median</b>	<b>3180</b>	<b>3255</b>	<b>0.537</b>
<b>range</b>	<b>2610-3440</b>	<b>2240-4070</b>	
<b>Apgar 1 min</b>			
<b>median</b>	<b>0</b>	<b>2<sup>+</sup></b>	<b>0.029§</b>
<b>range</b>	<b>0-1</b>	<b>1-7</b>	
<b>Apgar 10 min</b>			
<b>median</b>	<b>4</b>	<b>5<sup>+</sup></b>	<b>0.673</b>
<b>range</b>	<b>1-6</b>	<b>0-8</b>	
<b>Umbilical art pH</b>			
<b>median</b>	<b>6.83</b>	<b>7.28<sup>+</sup></b>	<b>0.019§</b>
<b>range</b>	<b>6.7-6.99</b>	<b>7.23-7.32</b>	
<b>Lactate mmol/l</b>			
<b>median</b>	<b>17</b>	<b>16<sup>+</sup></b>	<b>0.596</b>
<b>range</b>	<b>16-21</b>	<b>3-21</b>	
<b>Time of death after birth (h)</b>			
<b>median</b>	<b>44</b>	<b>13<sup>+</sup></b>	<b>0.143</b>
<b>range</b>	<b>20-171</b>	<b>1-672</b>	
<b>Res score*</b>			
<b>median</b>	<b>6</b>	<b>6<sup>+</sup></b>	<b>0.600</b>
<b>range</b>	<b>5-6</b>	<b>5-6</b>	
<b>Gender n (%)</b>			
<b>female</b>	<b>1 (20)</b>	<b>3 (50)</b>	<b>0.545</b>
<b>male</b>	<b>4 (80)</b>	<b>3 (50)</b>	
<b>Secondary apnea n (%)</b>	<b>5 (100)</b>	<b>1 (20)<sup>+</sup></b>	<b>0.047§</b>
<b>Seizures n (%)</b>	<b>4 (80)</b>	<b>0(0)<sup>+</sup></b>	<b>0.048§</b>





**A****B**

**A****B****C****D****E**

**A****B****C****D**